Journal of Neurochemistry, 2007, **101**, 682–696 doi:10.1111/j.1471-4159.2006.04341.x

Biochemical characterization of human glutamate carboxypeptidase III

Klára Hlouchová,*,† Cyril Bařinka,*,[1] Vojtěch Klusák,* Pavel Šácha,*,† Petra Mlčochová,*,† Pavel Majer,‡ Lubomír Rulíšek* and Jan Konvalinka*,†

*Institute of Organic Chemistry and Biochemistry, Academy of Sciences of the Czech Republic, Prague, Czech Republic
†Department of Biochemistry, Faculty of Natural Science, Charles University, Prague, Czech Republic
‡MGI Pharma Inc., Baltimore, Maryland, USA

Abstract

Human glutamate carboxypeptidase II (GCPII) is a transmembrane metallopeptidase found mainly in the brain, small intestine, and prostate. In the brain, it cleaves *N*-acetyl-L-aspartyl-glutamate, liberating free glutamate. Inhibition of GCPII has been shown to be neuroprotective in models of stroke and other neurodegenerations. In prostate, it is known as prostate-specific membrane antigen, a cancer marker. Recently, human glutamate carboxypeptidase III (GCPIII), a GCPII homolog with 67% amino acid identity, was cloned. While GCPII is recognized as an important pharmaceutical target, no biochemical study of human GCPIII is available at present. Here, we report the cloning, expression, and characterization of recombinant human GCPIII. We show that GCPIII lacks dipeptidylpeptidase IV-like activity, its activity is dependent on *N*-glycosylation, and it is effectively inhibited by several known inhibitors of GCPII. In comparison to GCPII, GCPIII has lower *N*-acetyl-L-aspartyl-glutamate-hydrolyzing activity, different pH and salt concentration dependence, and distinct substrate specificity, indicating that these homologs might play different biological roles. Based on a molecular model, we provide interpretation of the distinct substrate specificity of both enzymes, and examine the amino acid residues responsible for the differences by site-directed mutagenesis. These results may help to design potent and selective inhibitors of both enzymes.

Keywords: folate hydrolase, metallopeptidase, molecular modeling, *N*-acetylated-alpha-linked-acidic dipeptidase II, neurodegeneration, prostate-specific membrane antigen.
J. Neurochem. (2007) **101**, 682–696.

Glutamate carboxypeptidase II (GCPII, EC 3.4.17.21), also known as *N*-acetylated-alpha-linked-acidic dipeptidase (NAALADase), is a type-II transmembrane metallopeptidase found in a variety of human tissues, primarily in the central nervous system, small intestine, and prostate (Israeli *et al.* 1994; Troyer *et al.* 1995; Silver *et al.* 1997; Chang *et al.* 1999; Renneberg *et al.* 1999; Sokoloff *et al.* 2000). In the brain, it hydrolyzes the peptide neurotransmitter *N*-acetyl-L-aspartyl-glutamate (NAAG), thus liberating free glutamate (Robinson *et al.* 1987). Inhibition of GCPII has been shown to be neuroprotective in animal models of stroke, neuropathic pain and other neurodegenerative states (Slusher *et al.* 1999; Harada *et al.* 2000; Zhang *et al.* 2002; Ghadge *et al.* 2003), and thus it is being considered and tested as a potential therapeutic target (Subasinghe *et al.* 1990; Jackson *et al.* 1996; Nan *et al.* 2000; Whelan 2000; Neale *et al.* 2005; Tsukamoto *et al.* 2005; Zhou *et al.* 2005). In the small intestine, GCPII has been shown to facilitate the absorption

Received August 31, 2006; revised manuscript received October 26, 2006; accepted November 3, 2006.

Address correspondence and reprint requests to Jan Konvalinka, Institute of Organic Chemistry and Biochemistry, Academy of Sciences of the Czech Republic, Flemingovo n. 2, 166 10 Praha 6, Czech Republic. E-mail: konval@uochb.cas.cz
[1]The present address of Cyril Bařinka is the Center for Cancer Research, NCI, Frederick, MD 21702, USA.

Abbreviations used: β-NAAG, *N*-acetyl-L-aspartyl-β-linked L-glutamate; 2-PMPA, 2-phosphonomethyl-pentanedioic acid; AccQ, 6-aminoquinolyl-*N*-hydroxysuccinimidyl carbamate; DPP IV, dipeptidyl peptidase IV; HPLC, high-performance liquid chromatography; KO, knock-out; MD, molecular dynamics; MOPS, 3-[*N*-morpholino]propanesulfonic acid; NAAG, *N*-acetyl-L-aspartyl-L-glutamate; NAALADase, *N*-acetylated-alpha-linked-acidic dipeptidase; OPA, *o*-phthaldialdehyde; rhGCP, recombinant human glutamate carboxypeptidase; RMSD, root mean square deviation; SASA, solvent accessible surface area.

of folates by cleaving off the terminal glutamate from poly-gamma-glutamated folates (Pinto *et al.* 1996). In prostate, the physiological role of GCPII is unknown. However, as its expression increases significantly in prostate cancer, it is used as a prostate cancer diagnostic marker (prostate-specific membrane antigen) (Murphy *et al.* 1995; Gregorakis *et al.* 1998; Xiao *et al.* 2001; Schmidt *et al.* 2003).

The notion that GCPII hydrolyzes NAAG *in vivo* was based entirely on cellular response following the application of GCPII inhibitors. To test whether or not GCPII is the only protein with NAAG-hydrolyzing activity, two different groups constructed GCPII knock-out (KO) mice (Bacich *et al.* 2002; Tsai *et al.* 2003). While Tsai *et al.* reported that the deletion of GCPII gene in mice is lethal with embryos failing to develop past mid-term, Bacich *et al.* showed that GCPII KO mice develop normally to adulthood and exhibit a normal range of neurological responses and behaviors.

The results of Bacich *et al.* (2002) suggest that another NAAG-hydrolyzing enzyme might compensate for the missing activity of GCPII. Furthermore, Bacich *et al.* report that two potent inhibitors of GCPII inhibited the NAAG peptidase activity in the brains of GCPII KO mice, in which no GCPII was detected immunochemically. Therefore, the existence of a not-yet-identified GCPII homolog, which would compensate for the missing activity, was suggested.

In 1999, Pangalos *et al.* cloned two novel human peptidases, which are closely related to GCPII – NAALADase II [glutamate carboxypeptidase III (GCPIII)] and NAALADase L (Pangalos *et al.* 1999). While NAALADase L was unable to hydrolyze NAAG in transient transfection experiments, transient transfection of GCPIII cDNA confers NAAG-hydrolyzing activity to COS cells, just as had been shown for GCPII. The amino acid sequence of GCPIII was calculated to be 67% identical and 81% similar to that of GCPII (Pangalos *et al.* 1999) (see Fig. 1). The physiological role of this enzyme is unknown. Expression studies using RT-PCR and northern blot hybridization show that GCPIII mRNA is highly expressed in ovary and testes as well as within discrete brain areas (Pangalos *et al.* 1999). As there is no antibody specific to GCPIII available, the expression of the enzyme in various tissues is not known.

Glutamate carboxypeptidase II is increasingly recognized as an important potential pharmaceutical target. However, a detailed biochemical study of its closely related homolog GCPIII is still missing. So far, only mouse GCPIII has been cloned and partially characterized (Bzdega *et al.* 2004). It was reported that Chinese hamster ovary cells transfected with rat GCPII or mouse GCPIII expressed NAAG-hydrolyzing activity with similar V_{max} and K_M values (although V_{max} comparison is not very significant, as levels of protein expression by the transfected cells were not known). GCPIII mRNA levels were similar in brains obtained from wild-type mice and GCPII KO mice. Two potent inhibitors of GCPII, 2-phosphonomethyl-pentanedioic acid (2-PMPA, see Table 3) and FN6 (4,4′-phosphinicobis-butane-1,3 dicarboxylic acid), inhibit the NAAG peptidase activity in the brains of GCPII KO mice. Furthermore, it was shown that they are similarly potent inhibitors of rat GCPII and mouse GCPIII. The authors concluded that the nervous system cells express at least two homologous enzymes with similar pharmacological properties and affinity for NAAG (Bzdega *et al.* 2004). However, careful enzymatic characterization of GCPIII and its direct comparison with GCPII have not been provided.

In this article, we set out to analyze a human GCPII homolog on a molecular level to establish whether or not it could contribute to the NAAG-hydrolyzing activity and whether or not current GCPII inhibitors are able to block this activity completely. To this end, we present the expression, purification, and enzymologic characterization of human GCPIII, analysis of its substrate specificity, pH and ionic strength dependence and homology modeling followed by molecular dynamic simulations of its 3D structure, based on the recently solved 3D structure of human GCPII (Davis *et al.* 2005; Mesters *et al.* 2006).

Experimental procedures

Cloning of recombinant human glutamate carboxypeptidase III

Three different clones (EHS 1001-6454448, IHS 1382-8426921, MHS 1010-7508719), containing either partial or full-length GCPIII cDNA were purchased from Open Biosystems (Huntsville, AL, USA) and plasmid DNA was isolated from individual bacterial cultures. Subsequent sequencing revealed that the IHS1382 clone contained full-length GCPIII cDNA with no mutations and frameshifts, in contrast to the information found in the Open Biosystems database (http://www.openbiosystems.com). This clone was therefore used as a template for PCR reactions.

To clone the extracellular part of GCPIII (amino acids 36–740), the cDNA isolated from the IHS1382 clone was PCR-amplified using the primer pair FNAIIEXST (5′-AAAGGATCCGAAACGACCACTT-CTGTGCGCTATCATC-3′) and RNAII (5′-TTTCTCGAGCTATAA-TACTTCTTTCAGAGTTCCTGCTG-3′), with 30 cycles of: 94°C, 30 s; 63°C, 30 s; and 72°C, 4 min. The resulting PCR product was cloned into *Bgl*II/*Xho*I sites in the pMT/BiP/V5-HisA plasmid (Invitrogen, San Diego, CA, USA) in frame with the BiP signal sequence for extracellular secretion, and the expression plasmid was designated pMTBiP_NAIIexst. The sequence of the recombinant construct was subsequently verified by DNA sequencing.

Construction of rhGCPII(N519S) and rhGCPIII(S519N) mutants

Mutations N519S and S509N were introduced into pMTNAEXST (Barinka *et al.* 2002) and pMTBiP_NAIIexst, respectively, using the QuikChange Site-Directed Mutagenesis Kit (Stratagene,La Jolla, CA, USA). Primers of the following nucleotide sequence were used for the mutagenesis: FNAIN519S (5′-GCAAATTGGGATCT-GGAAGTGATTTTGAGGTGTTCTTCC-3′) and RNAIN519S (5′-GGAAGAACACCTCAAAATCACTTCCAGATCCCAATTTGC-3′)

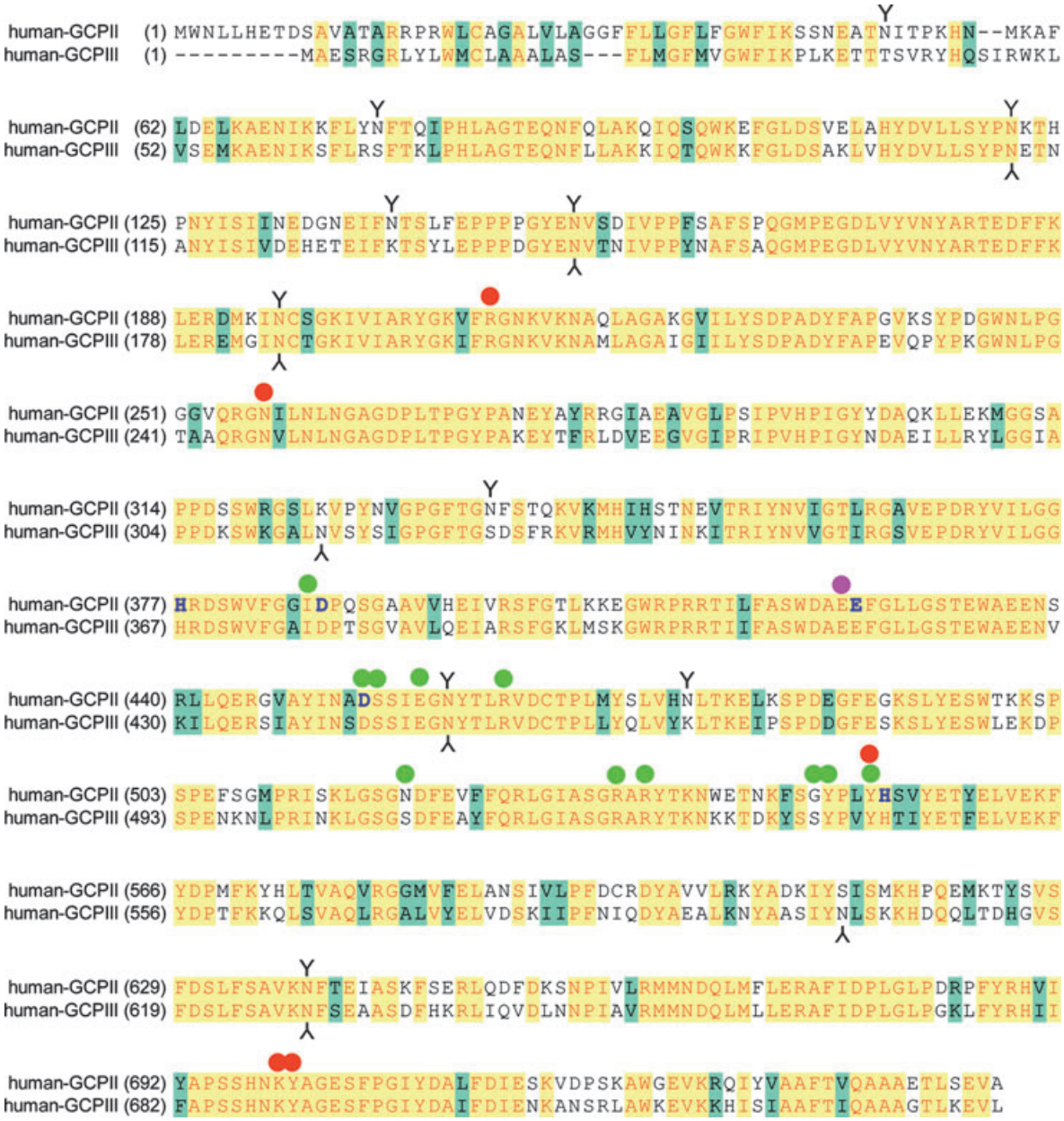

Fig. 1 Alignment of the human GCPII (E.C. 3.4.17.21) and GCPIII protein sequences (using clustal method with PAM250 residue weight table; gap penalty 3). Green ball: proposed residues interacting with the glutamate residue of the substrate in the S1 pocket; red ball: proposed residues interacting with the glutamate residue of the substrate in the S1′ pocket; purple ball: proposed proton shuttle catalytic base; blue residue symbol: zinc ligands; Y: potential *N*-glycosylation sites (Mesters *et al.* 2006).

for construction of recombinant human GCPII (rhGCPII) (N509S); FNAIIS509N (5′-CAATAAGCTGGGATCTGGAAATGACTTTG-AAGCTTATTTTC-3′) and RNAIIS519N (5′-GAAAATAAGCTT-CAAAGTCATTTCCAGATCCCAGCTTATTG-3′) for construction of rhGCPIII (S509N). The sequences of the recombinant constructs were subsequently verified by DNA sequencing.

The mutant recombinant proteins, designated rhGCPII(N519S) and rhGCPIII (S509N), were expressed in *Drosophila* Schneider's S2 cells and partially purified analogically to rhGCPIII as described below.

Stable transfection of *Drosophila* S2 cells

The *Drosophila* Schneider's S2 cells were grown in SF900II medium (Gibco, Rockville, MD, USA) until they reached a density of 2–4 × 10^6 cells/mL. The transfection was performed using the calcium phosphate transfection kit (Invitrogen) using 1 μg of pCoHYGRO DNA and 19 μg of pMTBiP_NAIIexst. The calcium phosphate solution was removed 16 h post-transfection and fresh SF900II medium supplemented with 10% fetal bovine serum was added (a complete medium). The cells were grown for one additional day and then the medium was replaced with the complete

medium containing 300 μg/mL Hygromycin B (Invitrogen). The selection medium was changed every 4–5 days. Extensive cell death of non-transfected cells was evident after about 1 week, and cells resistant to Hygromycin B started to grow out 3–4 weeks post-transfection.

Recombinant human GCPIII expression and purification

Large-scale expression of rhGCPIII in SF900II medium was carried out essentially as previously described for the rhGCPII construct (Barinka *et al.* 2002). Following cell harvest by centrifugation (500 *g* for 10 min), the conditioned medium was dialyzed 3× for 12 h at 4°C against 10 vols of 20 mmol/L 3-[*N*-morpholino]propanesulfonic acid (MOPS), 20 mmol/L NaCl, pH 6.5. The dialyzed medium was mixed with QAE-Sephadex A50 (6 g/L media, Pharmacia, New York, NY, USA) pre-equilibrated in 20 mmol/L MOPS, pH 6.5 (buffer A). The resulting slurry was stirred for 40 min at 24°C and filtered through a sintered glass filter. The retained QAE-Sephadex was washed with 100 mL buffer A. The pooled flow-through fractions were centrifuged at 15 000 *g* for 10 min at 4°C, filtered through a 0.22 μm filter, and applied onto a Source 15S column (HR10/10, Pharmacia) pre-equilibrated with buffer A at 24 °C. The rhGCPIII was eluted with a linear 0–0.5 mol/L NaCl gradient in buffer A. The fractions containing rhGCPIII were pooled, mixed with an equal volume of 100 mmol/L Tris–HCl, 0.8 mol/L NaCl, 2 mmol/L $CaCl_2$, 2 mmol/L $MnCl_2$, pH 7.4, and loaded onto a Lentil Lectin-Sepharose (Amersham Biosciences, Uppsala, Sweden) column (C10/10, Pharmacia) equilibrated with 20 mmol/L Tris–HCl, 0.5 mol/L NaCl, 1 mmol/L $CaCl_2$, 1 mmol/L $MnCl_2$, pH 7.4 at 4°C. The column was washed extensively, and rhGCPIII was eluted with 20 mmol/L Tris–HCl, 0.5 mol/L NaCl, 0.3 mol/L α-methyl-D-mannoside (Sigma, Praha, Czech Republic), pH 7.4. Fractions containing rhGCPIII were concentrated to a final volume of 2–3 mL using Centriprep YM-50 filters (Millipore, Billerica, MA, USA) and loaded onto a Superdex HR200 column (16/60; Pharmacia) pre-equilibrated with 20 mmol/L MOPS, 100 mmol/L NaCl, pH 7.4. The column was operated by AKTAExplorer FPLC system (AP Biotech, Little Chalfont, UK). Proteins were separated at a flow-rate of 0.5 mL/min and absorbance was monitored at 280 nm. The final protein preparation was concentrated to approximately 200 μg/mL and stored at −70°C until further use.

During purification, rhGCPIII was tracked by sodium dodecyl sulfate–polyacrylamide gel electrophoresis, western blot and radioenzymatic activity assay (see below).

Recombinant human GCPII expression and purification

The extracellular part of human GCPII, which spans amino acids 44–750, was cloned into the pMT/BiP/V5-His A plasmid (Invitrogen), and the recombinant protein (designated rhGCPII) was expressed in *Drosophila* Schneider's S2 cells and purified as described previously (Barinka *et al.* 2002).

Recombinant human GCPII and GCPIII carboxypeptidase activity determination

Radioenzymatic assay

Radioenzymatic assays using ^{3}H-NAAG (radiolabeled on the terminal glutamate) were performed as described previously (Robinson *et al.* 1987), with minor modifications (Barinka *et al.* 2002). Briefly, 20 mmol/L MOPS, 20 mmol/L NaCl, pH 7.4 (if not stated otherwise) and 10 μL of enzyme solution were pre-incubated for 5 min at 37°C in a final volume of 180 μL. About 20 μL mixture of 0.95 μmol/L 'cold' NAAG (Sigma) and 50 nmol/L ^{3}H-NAAG (50 Ci/mmol in Tris buffer, Perkin–Elmer, Wellesley, MA, USA) were added to each tube and incubation continued for 20 min. The reaction was stopped with 200 μL ice-cold 200 mmol/L sodium phosphate, pH 7.4; free glutamate was separated from the unreacted substrate by ion exchange chromatography, and quantified by liquid scintillation. If not stated otherwise, two duplicate reactions were performed for each measurement.

HPLC assay

Enzymatic reactions were performed in 20 mmol/L MOPS, 20 mmol/L NaCl, pH 7.4 (if not stated otherwise) in a total reaction volume of 120 μL. After incubation for 20 min at 37°C, the reaction was stopped by 60 μL 33 mmol/L EDTA, 66 mmol/L sodium borate, pH 9.2; and the released amino acids were derivatized using 20 μL of 6-aminoquinolyl-*N*-hydroxysuccinimidyl carbamate (AccQ)-Fluor reagent (Waters, Milford, NH, USA) dissolved in acetonitrile. An amount of 50 μL of the resulting mixture was applied to a Luna C18(2)-column (250 × 4.6 mm, 5 μm, Phenomenex, Torrance, CA, USA) mounted to a Waters Aliance 2795 system equipped with a Waters 2475 fluorescence detector and the products were separated using a 20–100% gradient of buffer B (60% acetonitrile, 40% buffer A) in buffer A (140 mmol/L sodium acetate, 17 mmol/L triethanolamine pH 5.05). The run time was 10 min.

Detection of reaction products by o-phthaldialdehyde modification

80mg *o*-phthaldialdehyde (OPA) (Sigma) was dissolved in 500 μL methanol and transferred into 40 mL of 0.8 mol/L sodium borate, pH 10.0, containing 90 mg *N*-acetyl cysteine (Sigma). This OPA solution (100 μL) was added to an equal volume of the reaction mixtures, vortexed, and left at 24 °C for 10 min. Fluorescence was measured on a Perkin–Elmer LS-3B fluorimeter (excitation at 330 nm, emission at 450 nm). If not stated otherwise, two duplicate reactions were performed for each measurement.

Screening of potential substrates

The substrates of general formulae Ac-X-Glu-OH or Ac-Asp-X-OH were prepared by solid phase peptide synthesis on a 2-chlorotrityl-chloride resin (Novabiochem, Darmstadt, Germany) as described previously (Barinka *et al.* 2002).

The individual compounds from the above-mentioned libraries were dissolved in 10% aqueous dimethylsulfoxide (Sigma). An amount of 10 μL of the enzyme (final concentration approximately 4.5 μg/mL, for rhGCPII reaction with Ac-Asp-Glu-OH and Ac-Glu-Glu-OH 0.45 μg/mL) was added to the buffered substrate solutions in a total volume of 100 μL (100 μmol/L individual compound, 20 mmol/L MOPS, 20 mmol/L NaCl pH 7.4). The reactions were allowed to proceed for 1 h at 37°C (the substrate conversion did not exceed 20%), stopped by the addition of 100 μL OPA solution and analyzed spectrofluorimetrically as described above.

The hydrolysis of all substrates from the libraries containing Pro or Lys was inspected by amino acid analysis on Biochrom 20 (Pharmacia Biotech, Uppsala, Sweden). About 100 μL reactions in

20 mmol/L MOPS, 20 mmol/L NaCl, pH 7.4 with 1 mmol/L substrate and 63 μg/mL enzyme concentrations were allowed to react for 1 h at 37°C. Hydrolysis of Ac-Pro-Glu-OH and Ac-Lys-Glu-OH was also determined by high-performance liquid chromatography (HPLC) as described above. A final enzyme concentration of approximately 3.4 μg/mL in 20 mmol/L MOPS, 20 mmol/L NaCl, pH 7.4 was reacted with 100 μmol/L substrate for 20 min at 37°C in a final volume of 120 μL (the substrate conversion did not exceed 5%).

Determination of kinetic parameters for NAAG, β-NAAG, and Ac-Glu-Glu-OH

The kinetics of substrate hydrolysis were determined by HPLC assay [NAAG, *N*-acetyl-L-aspartyl-β-linked L-glutamate (β-NAAG), and Ac-Glu-Glu-OH] and/or radiometric assay (NAAG), as described above. Typically, nanomolar enzyme concentrations were used to hydrolyze 0.4–400 μmol/L substrate in 20 mmol/L MOPS, 20 mmol/L NaCl, pH 7.4 (if not stated otherwise) for 20 min at 37°C. The substrate conversion did not exceed 20% and a total of 8–12 substrate concentration points were used for each determination.

pH Dependence of rhGCPII and rhGCPIII NAAG-hydrolyzing activity

To measure the pH dependence profile, the following selection of 20 mmol/L buffer, 10 mmol/L NaCl was used: citrate pH 4.0–5.0, 2-morpholinoethanesulfonic acid pH 5.0–6.5, MOPS 6.5–8.5, *N*-cyclohexyl-2-aminoethanesulfonic acid 8.5–10, *N*-cyclohexyl-3-aminopropanesulfonic acid 10–11. The profile was measured by fluorescence of products modified by OPA and by radiometric assay as described above.

For the fluorimetric assay, 100 μmol/L NAAG was reacted with approximately 0.5 μg/mL rhGCPII or 5 μg/mL rhGCPIII in a total volume of 100 μL for 1 h at 37°C. For the radiometric assay, reactions contained approximately 30 ng/mL of rhGCPII or 200 ng/mL of rhGCPIII and 100 nmol/L NAAG and proceeded for 20 min at 37°C.

Dependence of rhGCPII and rhGCPIII NAAG-hydrolyzing activity on NaCl concentration

The effect of NaCl concentration on rhGCPII and rhGCPIII enzyme kinetics of NAAG-hydrolysis was measured at 20, 50, 100, and 150 mmol/L NaCl concentrations in 20 mmol/L MOPS, pH 7.4. The radiometric assay described above was used with nanomolar enzyme concentrations so that the substrate conversion did not exceed 20%.

Determination of inhibition constants

Recombinant human glutamate carboxypeptidase III (80 ng/mL) or rhGCPII (20 ng/mL) was pre-incubated with differing inhibitor concentrations in 20 mmol/L MOPS, 20 mmol/L NaCl, pH 7.4, for 15 min at 37°C in a final volume of 180 μL. The radiometric assay described above was then used to measure the activities. The IC_{50} values were determined from the plots of v_i/v_0 (the ratio of individual reaction rates to rate of uninhibited reaction) against the inhibitor concentration using GraFit (version 5.0.4; Erithacus Software Ltd, Horley, UK) and used for the calculation of K_I values by the Morrison's formula for competitive inhibitors (Morrison 1969).

Dipeptidylpeptidase IV-like activity

Dipeptidyl peptidase IV (DPP IV) activity of rhGCPIII and rhGCPII was determined by fluorescent analysis of the Gly-Pro-AMC hydrolysis on a GENios TECAN reader (excitation at 360 nm, emission at 465 nm). Assays were initiated by the addition of enzyme (final concentration of 50 μg/mL) to the buffered substrate solutions (100 μmol/L Gly-Pro-AMC, 150 mmol/L glycine, pH 8.5) in a total reaction volume of 100 μL and monitored for 22 h at 37°C. C6 rat glial cells (cell lysate, final protein concentration of 100 μg/mL) were used as a positive control (Kato *et al.* 1978; Sedo *et al.* 1998).

In parallel, DPP IV activity was analyzed on HPLC using a similar assay as for carboxypeptidase activity (described above). Reactions were initiated by addition of 10 μmol/L Gly-Pro-AMC to the enzyme solution (final enzyme concentration approximately 5 μg/mL) in 20 mmol/L MOPS, 20 mmol/L NaCl, pH 7.4 in a total reaction volume of 60 μL. After incubation for 20 min at 37°C, the reaction was stopped by 30 μL 33 mmol/L EDTA, 66 mmol/L sodium borate, pH 9.2. The fluorescence of AMC was inspected by excitation at 335 nm, emission at 450 nm.

Recombinant human GCPIII and GCPII deglycosylation

An amount of 1 μL of PNGase F (NEB, 1000 U/μL) was used to deglycosylate 6 μg of native rhGCPIII and rhGCPII in 20 mmol/L MOPS, 20 mmol/L NaCl, pH 7.4. The deglycosylation took place at 37°C for 15 h in total volume of 100 μL.

Mass spectrometry

Matrix-assisted laser desorption/ionization (MALDI) mass spectra of rhGCPIII and rhGCPII were inspected by MALDI-TOF spectrometer Reflex4 (Bruker Daltonics, Bremen, Germany) using sinapic acid (Sigma) as the matrix.

Molecular modeling of GCPIII

• Protein(s) setup. All molecular dynamics (MD) simulations were based on the 2.0-Å structure of GCP II complexed with the inhibitor, 2-(4-iodobenzylphosphonomethyl)-pentanedioic acid (RCSB Protein Data Bank accession number 2C6C) (Mesters *et al.* 2006). Prior to MD simulations, three missing loops (consisting of 12 amino acids in total, Thr334-Phe337, Trp541-Phe546, Lys655-Ser656) were added using the GCP II structure at 3.5 Å resolution as a template (Davis *et al.* 2005). Then, a total number of ~100 atoms not resolved in side chains (i.e., missing in the structure coordinate file) were added by leap module of AMBER 8 (Case *et al*. 2004), using standard libraries. Finally, hydrogen atoms were added to the crystal structure and the system was solvated in a truncated octahedral box. The positions of (i) all the hydrogen atoms, (ii) all non-hydrogen atoms added to the original crystal structure as described above and (iii) all atoms of solvent water molecules were then optimized by a 300-ps simulated annealing (i.e., MD simulation at varying temperature under constant volume and periodic boundary conditions; for a detailed protocol, see below) followed by a conjugate gradient energy minimization of their positions. We assumed the normal protonation state at pH 7 for all amino acids (i.e., Glu, Asp in their deprotonated – anionic – form, and Lys, Arg in the protonated – cationic – form). For the His residues, the protonation status was decided from a detailed study of the hydrogen-bond network around the residue and the solvent

accessibility. Thus, in GCP II, His 82, 347, 377, 553, and 573 were assumed to be protonated on the $N^{\delta 1}$ atom, His 112, 124, 295, 396, 475, 689, and 697 on the $N^{\varepsilon 2}$ atom, whereas His 345 and 618 were considered to be protonated on both nitrogens.

- The initial GCPIII structure was then obtained by a replacement of the respective amino acid residues, preserving the GCPII geometry of main chain atoms, and using the side chain templates from standard Amber library (leap module). The protonation states of histidines were assumed as follows: His 82, 377, 553, and 731 were assumed to be protonated on the $N^{\delta 1}$ atom, His 112, 134, 295, 625, 647, 689, and 697 on the $N^{\varepsilon 2}$ atom, whereas His 345 and 618 were considered to be protonated on both nitrogens. Finally, to improve a poor description of electrostatics in the local environment of binuclear zinc(II) site, the default Amber charges were replaced by the ESP-fitted ones for ~60 atoms comprising the active site – $Zn_2(His)_2(Asp)_2(Glu)(OH)$ system.
- Molecular dynamics simulations. All MD simulations have been carried out with AMBER 8 (Case *et al.* 2004) program, using the Cornell force field (all_amino03.in) (Cornell *et al.* 1995). For a solvation model, explicit TIP3P water molecules were used with the boundaries of the truncated octahedron 9.0 Å outside any atom of the protein (resulting in the $105 \times 105 \times 105$ Å box size, total number of ~73 000 atoms in the simulation). The simulated annealing protocol consisted of 45 ps of heating the system up to 370 K, 150 ps of constant temperature simulation at 370 K, and 105 ps cooling the system to 0 K (with the time step of 1.5 fs). A cut-off for the non-bond interactions of 8.0 Å was employed. The bonds involving hydrogens were kept fixed at their equilibrium values by the SHAKE algorithm and dielectric constant of 1.0 was used in all simulations. Each MD simulation was then followed by the minimization of the resulting structure with the solvent molecules removed, except for 10 Å solvation shell of the protein, yielding the final structures that we refer to in this work. During the minimization, no cut-off has been used for non-bond interactions.
- Structure analysis. The final equilibrium structures of the two proteins obtained from the MD simulations were compared with respect to the overall fold, root mean square deviation (RMSD), cavity volume and cavity polarity. The disposable volume around the ligand was estimated by the program SURFNET (Laskowski 1995) with the following parameters: calculating the gaps between protein and inhibitor with grid separation 1 Å, minimum and maximum radius for gap spheres being 1.2 and 20 Å, respectively. The cavity surface was visualized using Pymol (DeLano 2002) and colored according to the vacuum electrostatic potential. Change in polarity of the cavity surface was estimated by comparing the solvent accessible surfaces of the charged functional groups (Arg, Lys, Glu, Asp) in the cavity using vmd program suite (Humphrey *et al.* 1996).

Results

Cloning, expression, and purification of human GCPIII

Three clones containing the human GCPIII sequence were identified by search in the Open Biosystems database, and the clone IHS 1382-8426921, spanning the full-length cDNA for GCPIII, was used for subsequent cloning. The sequence coding for the predicted extracellular part of GCPIII (rhGCPIII, amino acids 36–740) was PCR-amplified and cloned into pMTBiP/V5-His A *Drosophila* expression vector, in frame with the BiP signal sequence that directs secretion of the protein into the medium. rhGCPIII was efficiently secreted by the stably transfected S2 cells, and the enzyme was purified from the conditioned medium using ion-exchange chromatography on QAE-Sephadex A50, ion-exchange chromatography on a Source 15S column, and affinity chromatography on Lentil Lectin-Sepharose, exploiting the predicted *N*-glycosylation of GCPIII for the purification (Barinka *et al.* 2004b). Finally, the protein was purified by gel filtration on a Superdex HR200 column. The final purity of the protein was higher than 70% with a yield of approximately 1 mg of rhGCPIII per liter of media (Fig. 2, panel d). The protein was recognized by monoclonal antibody GCP-04 (Fig. 2, panel c), which was raised against rhGCPII (Barinka *et al.* 2004a).

Activity and substrate specificity of rhGCPIII when compared with rhGCPII

The availability of pure, active rhGCPIII enabled detailed analysis of its substrate specificity in direct comparison with its homolog rhGCPII. A panel of dipeptides of general formulae Ac-X-Glu-OH and Ac-Asp-X-OH (X stands for any naturally occurring L amino acid) was used for the analysis of the specificity of rhGCPIII in the S1 and S1′ subsites (Barinka *et al.* 2002). Identical amounts of rhGCPII and rhGCPIII were used in the cleavage reaction (with the exception of Ac-Asp-Glu-OH and Ac-Glu-Glu-OH hydrolysis by rhGCPII, in which the enzyme was 10 times more diluted). The cleavage of the C-terminal amino acid was analyzed fluorimetrically using OPA derivatization, except for the substrates containing proline or lysine (those were analyzed by amino acid analysis and/or HPLC assay following product derivatization by an AccQ-Fluor reagent; hydrolysis of these substrates was normalized to the cleavage of NAAG, which was used as a control). The products of the dipeptide hydrolysis were detected as an increase in fluorescence at $\lambda(EX)/\lambda(EM) = 330/450$ nm. The results of the assays are summarized in Figs 2a and b.

In agreement with earlier studies reported by our laboratory, rhGCPII was found to cleave Ac-Asp-Glu-OH (NAAG) and Ac-Glu-Glu-OH more efficiently by at least one order of magnitude than other compounds in the tested peptide libraries. However, this was not the case for rhGCPIII. The hydrolysis of Ac-Asp-Glu-OH and Ac-Glu-Glu-OH seems to be significantly less efficient than for rhGCPII. Other substrates in the Ac-X-Glu-OH library are hydrolyzed with approximately equal rates by rhGCPII and rhGCPIII. In the Ac-Asp-X-OH library, rhGCPIII does not significantly hydrolyze any substrate except for NAAG under the conditions selected. In contrast, rhGCPII effectively hydrolyzes Ac-Asp-Ala-OH and Ac-Asp-Met-OH as well. To verify that the enzyme responsible for the hydrolysis

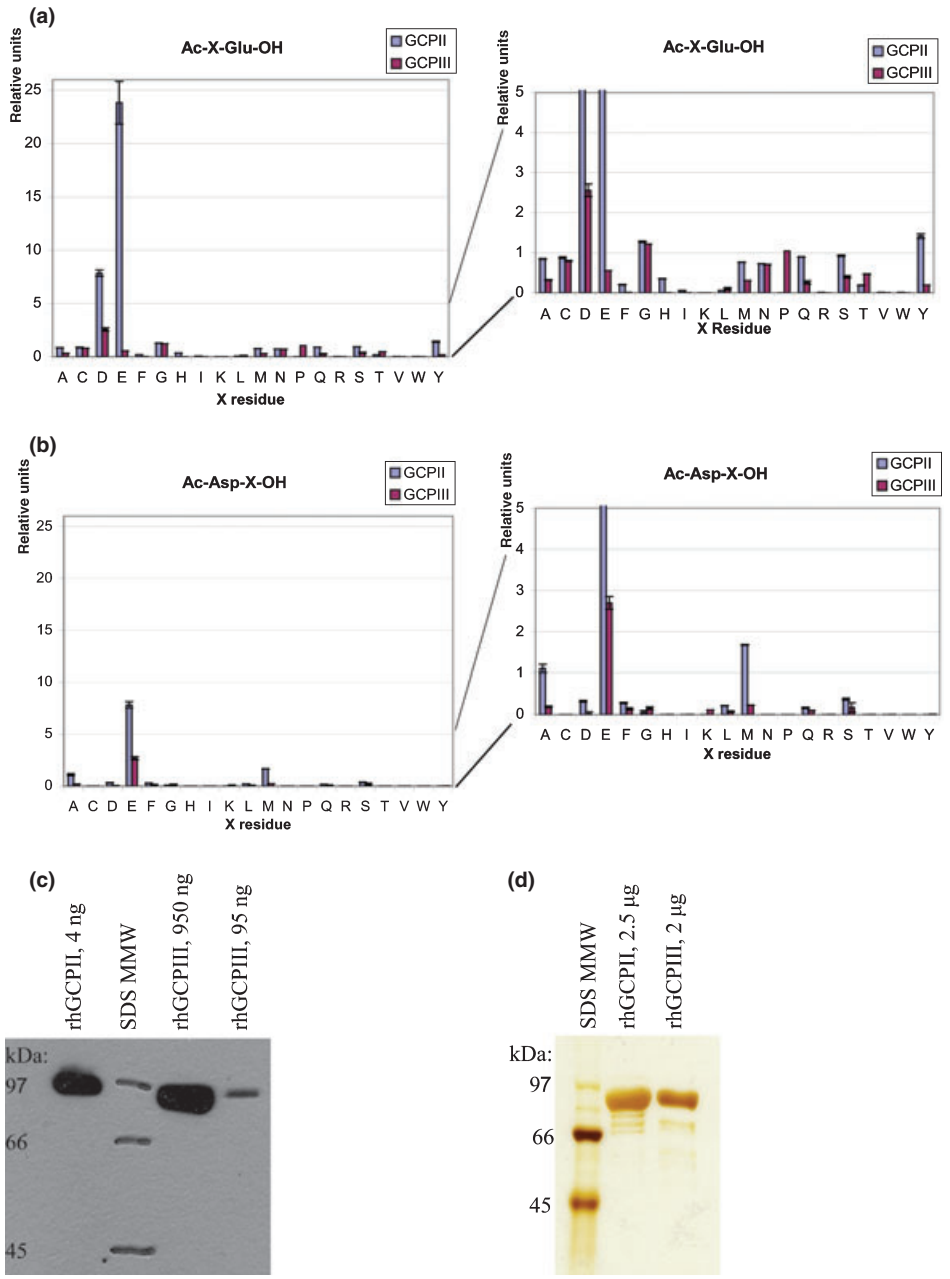

Fig. 2 Comparison of substrate specificities of rhGCPII and rhGCPIII in the P1 (panel a) and P1' (panel b) positions. Substrates of the general formula Ac-X-Glu-OH and Ac-Asp-X-OH (X standing for any naturally occurring amino acid except for Lys or Pro) were reacted with an enzyme (final concentration approximately 4.5 μg/mL, for rhGCPII reaction with Ac-Asp-Glu-OH and Ac-Glu-Glu-OH 0.45 μg/mL) and the products were detected spectrofluorimetrically after derivatization with *o*-phthaldialdehyde. Cleavage of the substrates containing Lys or Pro was analyzed by amino acid analysis and/or HPLC assay following product derivatization by an AccQ-Fluor reagent. Hydrolysis of these substrates was recalculated relative to NAAG, which was used as a control. On the right-hand side of both panels, the lower range (below 5 relative units) is expanded to allow for a better comparison between GCPII and GCPIII enzymatic activities against the less favored substrates. Panel c: western blot of purified rhGCPII and rhGCPIII with monoclonal antibody GCP-04. Indicated amounts of protein were resolved by 10% SDS–PAGE, electroblotted onto a nitrocellulose membrane, probed with the antibody GCP-04 and visualized by HRP-labeled anti-mouse antibody. Panel d: purity of rhGCPII and rhGCPIII. Indicated amounts of protein were resolved by 11% SDS–PAGE and visualized by silver staining.

Table 1 Direct comparison of NAAG, β-NAAG and Ac-Glu-Glu-OH hydrolysis by rhGCPII and rhGCPIII

	GCPII			GCPIII		
Substrate	K_M (nmol/L)	k_{cat} (per second)	k_{cat}/K_M [10^5/s/(mol/L)]	K_M (nmol/L)	k_{cat} (per second)	k_{cat}/K_M [10^5/s (mol/L)]
NAAG	1200 ± 500	1.1 ± 0.2	9.3 ± 4.9[ab]	370 ± 70	0.11 ± 0.01	3.0 ± 0.6[b]
Ac-Glu-Glu-OH	2600 ± 800	3.7 ± 0.4	14.1 ± 4.5[a]	3640 ± 1080	0.29 ± 0.02	0.8 ± 0.2[a]
β-NAAG	1400 ± 200	0.30 ± 0.01	2.1 ± 0.3[a]	5200 ± 1000	0.15 ± 0.01	0.3 ± 0.1[a]

Nanomolar enzyme concentrations were used to hydrolyze 0.4–400 μmol/L concentration of the analyzed substrate in 20 mmol/L MOPS, 20 mmol/L NaCl, pH 7.4. Enzyme kinetics of substrate hydrolysis was determined by HPLC assay [a](NAAG, β-NAAG and Ac-Glu-Glu-OH) and/or radiometric assay [b](NAAG).

reactions was rhGCPII/rhGCPIII rather than a host factor copurified with the enzyme (e.g., traces of *Drosophila* beta galactosidase protein, EC 3.2.1.23, were identified in the final rhGCPIII preparation by N-terminal sequencing), control reactions in the presence of the GCPII-specific inhibitor 2-PMPA (Jackson *et al.* 1996; Bzdega *et al.* 2004) were performed. No substrate hydrolysis was detected (data not shown).

Direct comparison of the enzymatic activity on cognate substrates was performed using NAAG, Ac-Glu-Glu-OH, and β-NAAG (refer to Pharmacological profile of rhGCPIII section). The substrates were cleaved by purified, titrated rhGCPII and rhGCPIII in 20 mmol/L MOPS, 20 mmol/L NaCl, pH 7.4 (see Experimental procedures section). The results are summarized in Table 1. The cleavage of the identified substrates by both enzymes follows Michaelis–Menten kinetics. The rhGCPIII K_M and k_{cat} constants for NAAG hydrolysis are 370 nmol/L and 0.11/s, respectively, suggesting that the catalytic efficiency of rhGCPIII for NAAG-hydrolysis is about threefold lower than that of rhGCPII in this particular set of conditions. The catalytic efficiency of rhGCPIII for Ac-Glu-Glu-OH is about 18-fold lower than that of rhGCPII.

DPP-IV-like activity of rhGCPII and rhGCPIII

Pangalos *et al.* (1999) reported a DPP-IV-like activity of COS cells transfected by GCPII and GCPIII cDNAs. We have previously shown (Barinka *et al.* 2002) that purified rhGCPII reveals no measurable hydrolysis of a typical fluorogenic substrate of DPP-IV, Gly-Pro-AMC (Kato *et al.* 1978; Sedo *et al.* 1998). Similarly, under the conditions described in the Experimental procedures section, we detected negligible DPP-IV-like activity (turnover lower than 0.01/s) using purified rhGCPIII.

Site-directed mutagenesis around the active site: NAAG-hydrolyzing activity of rhGCPII(N519S) and rhGCPIII(S509N)

In an effort to explain the differences in the proteolytic activities of rhGCPII and rhGCPIII, the amino acid residues of GCPII involved in the recognition of substrate/inhibitors [(Mesters *et al.* 2006) and Mlcochova *et al.*, unpublished data] were compared with the corresponding residues in the GCPIII protein sequence (see Fig. 1). The only noticeable difference between the two enzymes was the residue at position 519 (509 for GCP III), which is asparagine in GCPII and serine in GCPIII. As Asn519 has been proposed to bind the *N*-acetyl-aspartate part of NAAG (Mesters *et al.* 2006), recombinant proteins introducing the corresponding amino acid exchange in GCPII (N519S) and GCPIII (S509N) were cloned, expressed, and partially purified, and their NAAG-hydrolyzing activities were characterized. Results are summarized in Table 2. While mutation N519S of rhGCPII caused an approximately 10-fold decrease in K_M, the mutation S509N of rhGCPIII did not significantly change the value of K_M. Both mutations brought about a decrease in k_{cat} values in comparison with the wild-type proteins.

pH Dependence of rhGCPII and rhGCPIII

The pH dependence of NAAG hydrolysis by rhGCPII and rhGCPIII was measured in the pH range 4.0–11.0 at a saturating substrate concentration (100 μmol/L, by both the radiometric assay and fluorescence measurement using OPA derivatization, see Experimental procedures section for details) as well as at sub-K_M substrate concentration (100 nmol/L, the radiometric assay). The corresponding curves could thus be approximated as the pH dependence of k_{cat}/K_M (Fig. 3, panel a) and k_{cat} (panel b) for individual enzymes. rhGCPII shows a significant decrease in K_M

Table 2 Kinetic parameters for rhGCPII, rhGCPIII, rhGCPII(N519S) and rhGCPIII(S509N) NAAG hydrolysis

Recombinant protein	K_M (nmol/L)	k_{cat} (per second)	k_{cat}/K_M [10^5/s/ (mol/L)]
rhGCPII	1200 ± 500	1.1 ± 0.2	9.3 ± 4.9
rhGCPIII	370 ± 70	0.11 ± 0.01	3.0 ± 0.6
rhGCPII(N509S)	100 ± 30	0.42 ± 0.02	41 ± 12
rhGCPIII(S509N)	410 ± 110	0.026 ± 0.002	0.6 ± 0.2

NAAG hydrolysis was measured using the radiometric assay (see Experimental procedures section). Nanomolar enzyme concentrations were used to hydrolyze 0.4–400 μmol/L concentration of the analyzed substrate in 20 mmol/L MOPS, 20 mmol/L NaCl, pH 7.4.

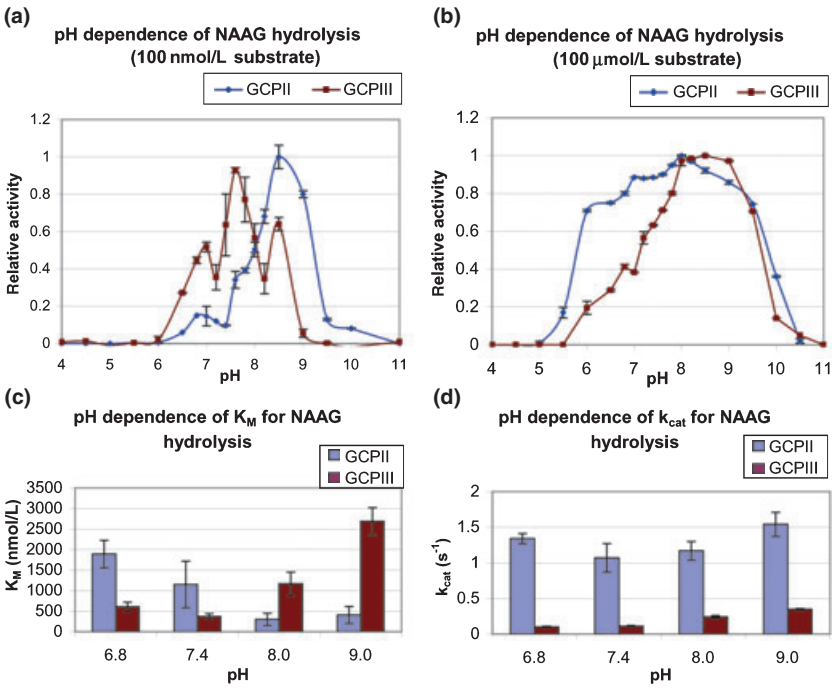

Fig. 3 pH dependence of rhGCPII and rhGCPIII NAAG-hydrolyzing activity. The pH dependence of NAAG hydrolysis by rhGCPII and rhGCPIII was measured using the following selection of 20 mmol/L buffer, 20 mmol/L NaCl: citrate pH 4.0–5.0, MES pH 5.0–6.5, MOPS 6.5–8.5, CHES 8.5–10, CAPS 10–11. Panels a and b: pH dependence curve for rhGCPII (blue) and rhGCPIII (red) measured with 100 nmol/L (panel a) and 100 μmol/L (panel b) substrate concentration. For the fluorimetric assay, 100 μmol/L NAAG was reacted with approximately 0.5 μg/mL rhGCPII or 5 μg/mL rhGCPIII. For the radiometric assay, reactions of less than 0.5 μg/mL enzyme with 100 nmol/L NAAG were used. The dependency curves were derived statistically from two independent measurements, each comprising of duplicate reactions. Panels c and d: kinetic constants (K_M, panel c; k_{cat}, panel d) of NAAG hydrolysis in pH values of 6.8, 7.4, 8.0 and 9.0. Enzyme kinetics of NAAG hydrolysis was determined by HPLC assay and/or radiometric assay. Nanomolar enzyme concentrations were used to hydrolyze 0.4–400 μmol/L concentration of the analyzed substrate. The substrate conversion did not exceed 20% and a total of 8–12 substrate concentration points measured in duplicates were used for single determination. Typically, two independent measurements were performed to determine an average value.

from pH 6.8 to 9.0, while the k_{cat} value over the pH region is almost constant. On the contrary, pH dependence values for rhGCPIII suggest a more acidic pH optimum for K_M (around 7.4; Fig. 3, panel c) and an apparent increase in k_{cat} value between pH 6.0 and 9.0 (Fig. 3, panels b and d). At selected pH values, the kinetic constants for NAAG-hydrolysis by the enzymes were determined. The overall catalytic efficiency optimum of rhGCPII is shifted to basic pH, compared with the optimum of rhGCPIII, which is around pH 7.4 (Fig. 3, panel a). Taken together, rhGCPIII shows a more pronounced pH dependence than rhGCPII and the difference in activities between rhGCPII and rhGCPIII increases with pH value.

Dependence of rhGCPII and rhGCPIII NAAG-hydrolyzing activity on salt concentration

The effect of NaCl on rhGCPII and rhGCPIII NAAG-hydrolyzing activity was assayed at concentrations of 20, 50, 100, and 150 mmol/L NaCl (Fig. 4). Interestingly, rhGCPII and rhGCPIII show opposite dependence of K_M on the NaCl concentration: while rhGCPII binds its substrate better in higher salt concentrations (a few fold decrease in the K_M value between 20 and 50 mmol/L NaCl), rhGCPIII has a higher affinity for NAAG at 20 mmol/L than at 50 mmol/L NaCl (Fig. 4a). The value of k_{cat} changes significantly only for rhGCPIII at the concentrations of NaCl tested (Fig. 4b), while the k_{cat} for GCPII remains nearly constant. The overall catalytic efficiency (expressed as k_{cat}/K_M) of NAAG hydrolysis is not significantly affected by NaCl concentration for rhGCPIII, while for rhGCPII it increases significantly from 20 to 150 mmol/L NaCl concentrations.

Pharmacological profile of rhGCPIII

As GCPIII activity was suggested to be a compensatory NAAG-hydrolyzing activity in GCPII KO mice (Bacich *et al.* 2002) and only limited data exists whether or not this homolog is inhibited by compounds targeting GCPII, we set out to directly compare the inhibition pattern of rhGCPIII and GCPII. To this end, we analyzed rhGCPIII inhibition by general metallopeptidase inhibitors (EDTA, 1,10-phenanthr-

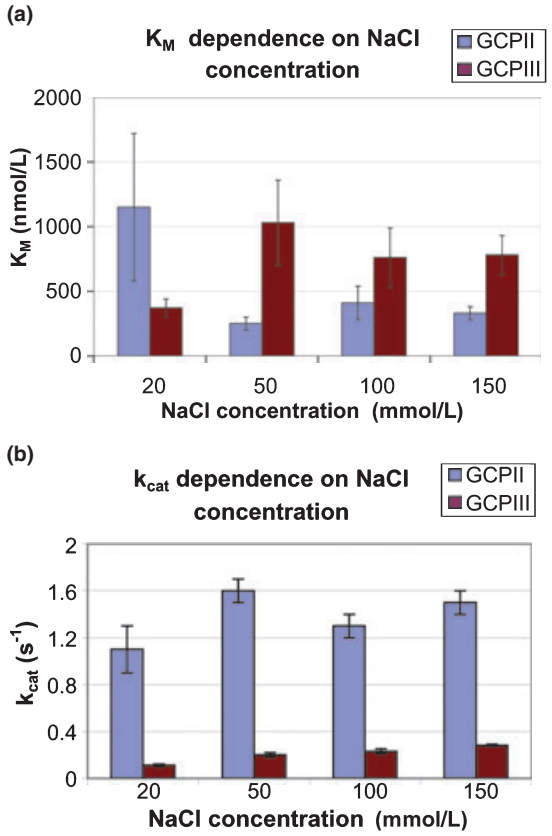

Fig. 4 Dependence of rhGCPII and rhGCPIII NAAG-hydrolyzing activity on NaCl concentration. Panels a and b: the effect of NaCl concentration on rhGCPII and rhGCPIII NAAG-hydrolyzing activity was measured in 20, 50, 100, and 150 mmol/L NaCl concentration in 20 mmol/L MOPS, pH 7.4. The radiometric assay described above was used with nanomolar enzyme concentrations so that the conversion of substrate did not exceed 20%.

oline), substrate analogs (β-NAAG), and phophonate, phosphinate- or thiol-based compounds designed as GCPII inhibitors (Jackson *et al.* 1996; Tsukamoto *et al.* 2002, 2005; Majer *et al.* 2003, 2006).

Consistent with the notion that GCPIII is a cocatalytic metallopeptidase and that its hydrolytic activity is metal-ion-dependent, all of the chelating agents tested completely abolished its proteolytic activity (data not shown). Surprisingly, β-NAAG, a conformational analog of NAAG that is reported to be a competitive inhibitor of GCPII with a K_I value of 0.7 μmol/L (Serval *et al.* 1990), turned out to be hydrolyzed by both rhGCPIII and rhGCPII quite efficiently. The cleavage of this 'substrate-inhibitor' by both enzymes follows Michaelis–Menten kinetics with kinetic constants K_M = 1.4 μmol/L, k_{cat} = 0.3/s and K_M = 5.2 μmol/L, k_{cat} = 0.15/s for rhGCPII and rhGCPIII, respectively (see Table 1).

To extend these inhibition studies, IC_{50} values for seven different inhibitors, originally designed as GCPII-specific inhibitors, were assessed using rhGCPII and III and the radioenzymatic assay. First, we determined that 2-PMPA is a competitive inhibitor of rhGCPIII with a K_I of 0.9 nmol/L, and this compound was subsequently used for the active-site titration of rhGCPIII (data not shown). The IC_{50} values for other inhibitors were then utilized for calculation of K_I values using Morrison's formula for competitive inhibitors (Morrison 1969), and the results are summarized in Table 3. Reflecting the sequence and likely structural (see below) similarity between rhGCPII and rhGCPIII, the potencies (i.e., K_I values) of all the compounds against the two peptidases are comparable. The only noticeable differences were observed for inhibition constants of inhibitors I-2 (RS), (S), and (R), which show several fold lower K_I values for rhGCPIII than rhGCPII. Additionally, it is interesting to note that the (*S*)-enantiomer of I-2, which has a stereochemical configuration analogous to L-glutamate of NAAG, is more potent in terms of rhGCPII/rhGCPIII inhibition than the corresponding (R)-form. This finding is consistent with GCPII (and supposedly GCPIII) preferences for L-amino acid-containing substrates as well as data for the inhibition constants of (R,S)-enantiomers of 2-PMPA (Robinson *et al.* 1987; Vitharana *et al.* 2002). Taken together, the pharmacological profiles for both NAAG-peptidases are quite similar and inhibitors designed against GCPII also effectively inhibit rhGCPIII activity. It could therefore be hypothesized that *in vivo* administration of GCPII/GCPIII inhibitors would completely abolish total NAAG-peptidase activity in the targeted area.

Mass spectrometry

The mass of the polypeptide backbone of both rhGCPII and rhGCPIII calculated from the known amino acid sequence is 79.8 kDa. Mass spectrometry analysis showed that the molecular weight of the recombinant glycosylated proteins rhGCPII and rhGCPIII is approximately 89.1 kDa in both cases. For both proteins, post-translational modifications represent approximately 9.3 kDa, while the number of potential *N*-glycosylation sites in GCPII and GCPIII is 10 and 7, respectively (Fig. 1).

Role of *N*-glycosylation

It has been shown for GCPII that its *N*-glycosylations are vital for the carboxypeptidase activity (Barinka *et al.* 2002, 2004b; Ghosh and Heston 2003). To determine the role of *N*-glycosylation on GCPIII activity, rhGCPIII was deglycosylated using PNGase F. Similarly to GCPII, deglycosylation of the native protein completely abolished its carboxypeptidase activity (data not shown).

Molecular modeling of GCPIII structure

As shown in Fig. 1, the amino acid sequence of GCPIII is 67% identical and 81% similar to that of GCPII. Such a high level of sequence similarity implies a high level of structural similarity. To analyze and interpret the differences in

Table 3 Comparative analysis of rhGCPII and rhGCPIII inhibition by specific inhibitors

Inhibitor	Molecular formula	K_i for rhGCPII (nmol/L)	K_i for rhGCPIII (nmol/L)
I-1	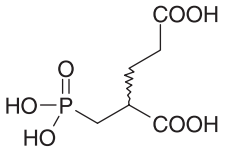	0.9 ± 0.2	0.8 ± 0.1
I-2 (RS)	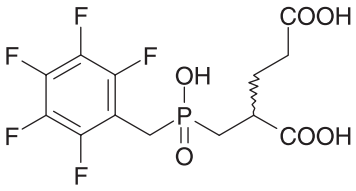	27 ± 9	8.1 ± 3.2
I-2 (S)		17 ± 4	2.0 ± 1.6
I-2 (R)		480 ± 140	120 ± 53
I-3	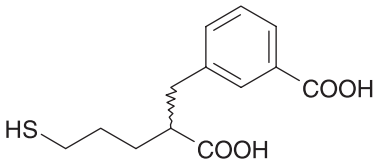	7.4 ± 2.9	15 ± 3
I-4	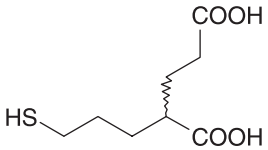	14 ± 6	58 ± 25
I-5	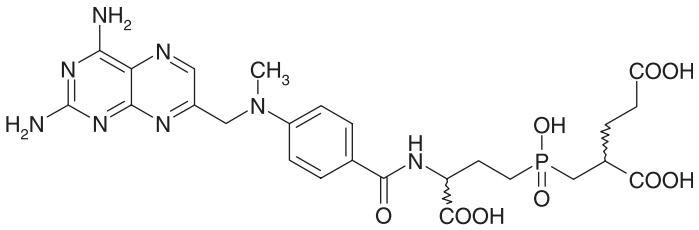	0.12 ± 0.03	0.35 ± 0.28

IC_{50} values were used for the calculation of K_i values using the Morrison's formula for competitive inhibitors (Morrison 1969). I-1 is a racemate form of 2-PMPA (Jackson *et al.* 1996), I-2(RS) is the racemate of 2-(hydroxy-pentafluorophenylmethyl-phosphinoylmethyl) pentanedioic acid, while I-2(S) and I-2(R) are its individual enantiomers [compounds RS-2, S-2 and R-2 from (Tsukamoto *et al.* 2005)]. Inhibitor I-3 is 3-(2-carboxy-5-mercapto-pentyl)-benzoic acid [compound 6c in (Majer *et al.* 2006)]. I-4 is 2-(3-mercaptopropyl)pentanedioic acid [compound 4d in (Majer *et al.* 2003)] and I-5 is a phosphinate analog of *N*-acylated γ-glutamylglutamate [compound 4 in (Tsukamoto *et al.* 2002)]. The radiometric assay was used (see Experimental procedures section).

enzymatic activities between GCPII and GCPIII, we constructed a model of the 3D structure of GCPIII as described in the Experimental procedures section.

The final equilibrium structures of the two proteins obtained from the MD simulations were compared with respect to the overall fold, RMSD, cavity volume and cavity polarity. The direct comparison of the GCPII and GCPIII structures is provided in Fig. 5, panel a. The figure shows a high structural similarity between the two homologous enzymes with an identical overall fold. The backbone RMSD

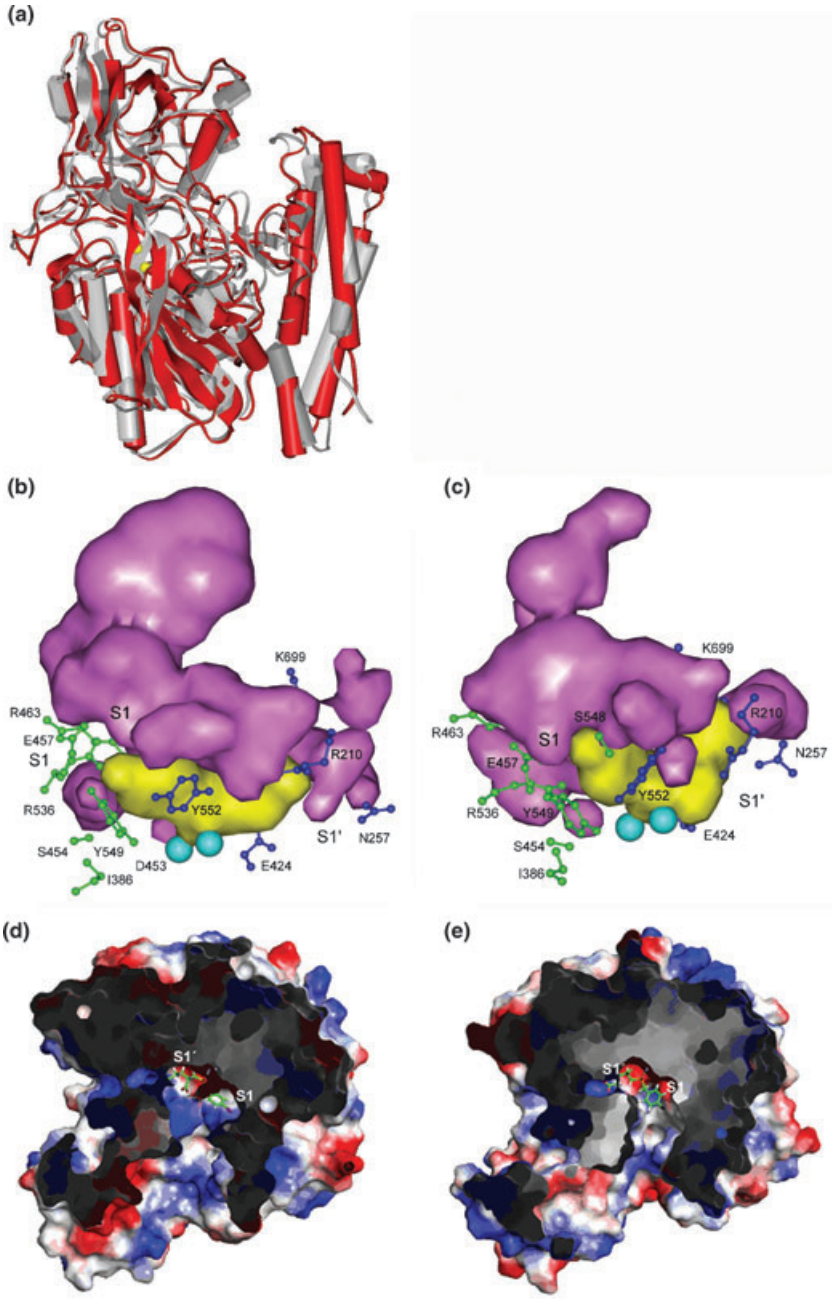

Fig. 5 Molecular model of GCPIII structure. Panel a: structural model of GCPIII (red) superimposed on the 3D structure of GCPII (gray) in complex with specific inhibitor (Mesters *et al.* 2006) as obtained from MD simulation (see Experimental procedures section for details). Catalytic zinc atoms depicted as yellow spheres. Panels b and c: comparison of active-site clefts of GCPII and GCPIII as seen from molecular modeling. Binding site cavities of GCPII (panel b) and GCPIII (panel c) as compared using program SURFNET. Yellow shows the inhibitor, 2-(4-iodobenzylphosphonomethyl)-pentanedioic acid, bound in the cavity; purple represents the remaining volume of the active-site cavity. The catalytic zinc atoms depicted as light blue spheres, S1 proposed residues in green, S1′ residues in blue. The volume of the cavity in GCPIII is smaller by roughly 30% in comparison with GCPII. Panels d and e: A cut through the surface of the GCPII (panel d) and GCPIII (panel e), colored according to the vacuum electrostatics potential in Pymol (DeLano 2002). The surfaces of the binding site cavities of GCPII and GCPIII are shown with charged residues depicted in blue (positive) and red (negative). Inhibitor 2-(4-iodobenzylphosphonomethyl)-pentanedioic acid bound in the cavity.

is 2.17 Å. While the overall fold is preserved in both enzymes, the structure of the substrate/inhibitor binding cavities of GCPII and III significantly differs. The differences are mainly in the size and shape of the cavities as well as in their surface charge. The change of cavity polarity is important as the native substrate of the enzymes, Ac-Asp-Glu, is negatively charged (formal charge -3). The effective charge could be quantified by measuring the solvent accessible surface area (SASA) of the charged groups exposed on the cavity surface. We have identified 15 charged residues on the cavity surface. All of them are preserved in the sequence of GCPIII and are mostly present in the cavity.

The prevailing charge on the surface of the cavity of GCPII is positive. The positive/negative surface ratio is 3.6 (151/42). In case of GCPIII, the positive charge also prevails but the ratio is only 1.7 (114/66) because of decrease in the positive SASA and, at the same time, increase in the negative SASA. Although the charged residues in the PR binding cavity are conserved, the conformation change leads to a considerable decrease in the positively charged surface and minor increase in the negatively charged surface (Fig. 5, panels d and e).

Our model also reveals a change in the shape of the substrate-binding pocket. The accessible volume between the

ligand and the protein is significantly smaller in the case of GCPIII in comparison to GCPII, representing a mere 68% of that in GCPII. (Fig. 5, panels b and c).

Discussion

Glutamate carboxypeptidase II is now becoming widely recognized as an important pharmaceutical target and a diagnostic tool for a number of pathologies ranging from neuropathy to prostate cancer. Therefore, its homologs with the potential to compensate for GCPII enzymatic activity or other potential functions represent a very relevant target of enzymologic research. In this report we analyze GCPIII, a homolog of human GCPII, and address the following questions: (i) what is the substrate specificity of GCPIII? (ii) how do the activities of the two enzymes relate? (iii) could GCPIII compensate for the activity of GCPII and could it be inhibited by the existing inhibitors designed against GCPII?

To answer the first question, a panel of dipeptides of general formulae Ac-X-Glu-OH and Ac-Asp-X-OH was used for direct comparison of the specificity of these two enzymes in the S1 and S1′ binding pockets (Barinka *et al.* 2002). As we reported earlier, rhGCPII shows a strong preference for Ac-Asp-Glu-OH (NAAG) and Ac-Glu-Glu-OH, and all other tested substrates (including Ac-Asp-Met-OH) are cleaved at least one order of magnitude less efficiently. In contrast, the substrate specificity of rhGCPIII seems to be less pronounced. While the other substrates in the libraries are cleaved with similar efficiencies by both enzymes, the cognate substrate, Ac-Asp-Glu-OH, is cleaved less effectively by rhGCPIII. Furthermore, in contrast to rhGCPII, rhGCPIII does not cleave Ac-Asp-Ala-OH and Ac-Asp-Met-OH.

To directly compare the catalytic efficiencies of the two enzymes, we determined the kinetic constants of the cleavage of the cognate substrate of GCPII, Ac-Asp-Glu-OH (NAAG), and of two other substrates, Ac-Glu-Glu-OH and β-NAAG. rhGCPIII hydrolyzed all three substrates less efficiently, but only in case of Ac-Glu-Glu-OH did this difference exceed one order of magnitude, suggesting thus different structural preferences for the amino acid occupying the P1 position of the substrate.

This measurement was performed at pH 7.4, which is arguably close to the environment of a neuronal synapse. However, for a meaningful activity comparison, optimal conditions for both enzymes (namely the pH and salt concentration optima) should also be considered, especially when the physiological activity and localization of GCPIII are not known.

An earlier study by Bzdega *et al.* (2004) shows that the pH dependencies of rat GCPII and mouse GCPIII NAAG-hydrolyzing activities are very similar. Nevertheless, the activity measurements were performed at only one substrate concentration, and the kinetic constants were not determined in their study. Moreover, the quantification of GCPII and GCPIII levels was difficult, as membranes from transfected cells were used in the assay. On the contrary, our measurements with purified rhGCPII and rhGCPIII reveal that the pH dependencies of these two closely homologous enzymes are strikingly different. The pH dependence of rhGCPII forms a typical bell-shaped curve with k_{cat} stable over the neutral and slightly basic region and K_M sharply decreasing with pH. In contrast, the pH optimum of rhGCPIII is shifted to the neutral region, it has a narrower maximum, and the K_M actually increases with pH in the pH range of 6.8–9.0. An interpretation of this dissimilarity can be derived from a structural model of GCPIII, which we constructed on the basis of a recently determined 3D structure of GCPII (Mesters *et al.* 2006). As the native substrates of GCPII are negatively charged, it is not surprising that the prevailing charge on the surface of GCPII's binding cavity is positive. Although the charged residues in the GCPIII binding cavity are conserved, the amino acid exchanges in the vicinity of the binding cavity lead to a considerable decrease in a positively charged surface area and a minor increase of the negatively charged surface in comparison to GCPII. As a result, the prevailing charge on the surface of the GCPIII binding cavity is less positive, which could account for the more acidic pH optimum for rhGCPIII than for rhGCPII. Similarly, this difference in positively charged surface area could have an impact on the substrate specificities of the two homologs.

The GCPII activity determinations reported in the literature have typically been performed in 50 mmol/L Tris buffer pH 7.4 with or without various salt concentrations. We demonstrate that for both enzymes, the kinetic parameters of NAAG hydrolysis can be significantly altered by salt concentration. While the K_M of rhGCPII reaches its minimum at 50 mmol/L NaCl and does not change significantly with increasing salt concentration up to 150 mmol/L NaCl, rhGCPIII has the highest affinity for NAAG at 20 mmol/L NaCl concentration. The k_{cat} value changes significantly only for rhGCPIII and increases with the NaCl concentration. These data are very important when the activities of GCPII and GCPIII are directly compared. For instance, in 20 mmol/L MOPS, 150 mmol/L NaCl, pH 7.4, the catalytic efficiency of rhGCPII is more than 10× higher than that of rhGCPIII, while in the same buffer with lower salt concentration (20 mmol/L NaCl, more relevant for intracellular compartments) this efficiency is only 3× higher.

The GCPII inhibitors analyzed in this article effectively block the peptidase activity of rhGCPIII. The prototype phosphonate-based inhibitor I-1 exhibits the same K_I against both enzymes, while the inhibitor I-2 with pentafluoro benzyl group in the P1 position is roughly three to eight times more potent against rhGCPIII. The potency increase seems to be slightly higher in the case of the more active enantiomer (I-2(S)). The pentafluoro benzyl group, which is situated at the

edge of the binding pocket and does not make any obvious contacts with the enzyme (Mesters *et al.* 2006) is better tolerated by GCPIII in comparison with rhGCPII. This is likely because of the lower overall positive charge of the surface of GCPIII, which repels the hydrophobic group less than the highly charged surface of GCPII. The situation is reversed in the case of thiol containing inhibitors I-3 and I-4 and the methotrexate-based inhibitor I-5, but here the differences in the values of K_I are not so significant. In addition to the change in polarity of the binding cavities, the structural model of GCPIII also reveals that the binding cavity of GCPIII is smaller than that of GCPII by approximately 30%. Implications of this difference on the geometry of the GCPIII binding cavity with respect to GCPII might also help to explain these differences in inhibitor binding.

Overall, the presented series of inhibitors, which were originally designed for GCPII, showed very similar activities against rhGCPIII regardless of their size and different zinc-binding groups. This finding is relevant in particular with respect to the potential use of GCPII inhibitors for treatment of disorders associated with glutamate excitotoxicity, as potent compounds should effectively block pathological release of glutamate caused by either of the two proteases.

In conclusion, the physiological substrate of GCPII, Ac-Asp-Glu-OH (NAAG), is also hydrolyzed by rhGCPIII but less efficiently and with significantly different pH and salt concentration optima. We believe that this GCPIII activity is significant enough to account for the NAAG-hydrolyzing activity observed in the tissues of GCPII KO mice (Bacich *et al.* 2002) and that GCPIII might thus represent a valid pharmaceutical target. We show on a panel of GCPII inhibitors that the pharmacologic profiles of the two homologs are quite similar. However, as the substrate specificities are distinct and the biological significance of GCPIII is not yet known, our findings might be used for the design of compounds selectively targeting either GCPII or GCPIII. Such inhibitors would be instrumental to evaluate and dissect biological roles of the two individual enzymes.

Acknowledgements

The authors thank Jana Starkova for excellent technical assistance, Martin Hradilek for peptide synthesis and Hillary Hoffman for language corrections and proofreading. Financial assistance of the Grant Agency of the Czech Republic (301/03/0784) and Ministry of Education of the Czech Republic (Research Centre for new Antivirals and Antineoplastics, 1M0508) is gratefully acknowledged.

References

Bacich D. J., Ramadan E., O'Keefe D. S. *et al.* (2002) Deletion of the glutamate carboxypeptidase II gene in mice reveals a second enzyme activity that hydrolyzes N-acetylaspartylglutamate. *J. Neurochem.* **83**, 20–29.

Barinka C., Rinnova M., Sacha P., Rojas C., Majer P., Slusher B. S. and Konvalinka J. (2002) Substrate specificity, inhibition and enzymological analysis of recombinant human glutamate carboxypeptidase II. *J. Neurochem.* **80**, 477–487.

Barinka C., Mlcochova P., Sacha P., Hilgert I., Majer P., Slusher B. S., Horejsi V. and Konvalinka J. (2004a) Amino acids at the N- and C-termini of human glutamate carboxypeptidase II are required for enzymatic activity and proper folding. *Eur. J. Biochem.* **271**, 2782–2790.

Barinka C., Sacha P., Sklenar J., Man P., Bezouska K., Slusher B. S. and Konvalinka J. (2004b) Identification of the N-glycosylation sites on glutamate carboxypeptidase II necessary for proteolytic activity. *Protein Sci.* **13**, 1627–1635.

Bzdega T., Crowe S. L., Ramadan E. R., Sciarretta K. H., Olszewski R. T., Ojeifo O. A., Rafalski V. A., Wroblewska B. and Neale J. H. (2004) The cloning and characterization of a second brain enzyme with NAAG peptidase activity. *J. Neurochem.* **89**, 627–635.

Case D. A., Darden T. A., Cheatham T. E. III *et al.* (2004) *AMBER 8*. University of California, San Francisco.

Chang S. S., Reuter V. E., Heston W. D., Bander N. H., Grauer L. S. and Gaudin P. B. (1999) Five different anti-prostate-specific membrane antigen (PSMA) antibodies confirm PSMA expression in tumor-associated neovasculature. *Cancer Res.* **59**, 3192–3198.

Cornell W. D., Cieplak P., Bayly C. I. *et al.* (1995) A second generation force field for the simulation of proteins, nucleic acids and organic molecules. *J. Am. Chem. Soc.* **117**, 5179–5197.

Davis M. I., Bennett M. J., Thomas L. M. and Bjorkman P. J. (2005) Crystal structure of prostate-specific membrane antigen, a tumor marker and peptidase. *Proc. Natl Acad. Sci. USA* **102**, 5981–5986.

DeLano W. L. (2002) *The PyMOL User's Manual*. DeLano Scientific, San Carlos, CA, USA.

Ghadge G. D., Slusher B. S., Bodner A. *et al.* (2003) Glutamate carboxypeptidase II inhibition protects motor neurons from death in familial amyotrophic lateral sclerosis models. *Proc. Natl Acad. Sci. USA* **100**, 9554–9559.

Ghosh A. and Heston W. D. (2003) Effect of carbohydrate moieties on the folate hydrolysis activity of the prostate specific membrane antigen. *Prostate* **57**, 140–151.

Gregorakis A. K., Holmes E. H. and Murphy G. P. (1998) Prostate-specific membrane antigen: current and future utility. *Semin. Urol. Oncol.* **16**, 2–12.

Harada C., Harada T., Slusher B. S., Yoshida K., Matsuda H. and Wada K. (2000) N-acetylated-alpha-linked-acidic dipeptidase inhibitor has a neuroprotective effect on mouse retinal ganglion cells after pressure-induced ischemia. *Neurosci. Lett.* **292**, 134–136.

Humphrey W., Dalke A. and Schulten K. (1996) VMD: visual molecular dynamics. *J. Mol. Graph.* **14**, 33–38.

Israeli R. S., Powell C. T., Corr J. G., Fair W. R. and Heston W. D. (1994) Expression of the prostate-specific membrane antigen. *Cancer Res.* **54**, 1807–1811.

Jackson P. F., Cole D. C., Slusher B. S., Stetz S. L., Ross L. E., Donzanti B. A. and Trainor D. A. (1996) Design, synthesis, and biological activity of a potent inhibitor of the neuropeptidase N-acetylated alpha-linked acidic dipeptidase. *J. Med. Chem.* **39**, 619–622.

Kato T., Nagatsu T., Kimura T. and Sakakibara S. (1978) Fluorescence assay of x-prolyl dipeptidyl-aminopeptidase activity with a new fluorogenic substrate. *Biochem. Med.* **19**, 351–359.

Laskowski R. A. (1995) SURFNET: a program for visualizing molecular surfaces, cavities, and intermolecular interactions. *J. Mol. Graph.* **13**, 323–328.

Majer P., Jackson P. F., Delahanty G. *et al.* (2003) Synthesis and biological evaluation of thiol-based inhibitors of glutamate carboxypeptidase II: discovery of an orally active GCP II inhibitor. *J. Med. Chem.* **46**, 1989–1996.

Majer P., Hin B., Stoermer D. *et al.* (2006) Structural optimization of thiol-based inhibitors of glutamate carboxypeptidase II by modification of the P1′ side chain. *J. Med. Chem.* **49**, 2876–2885.

Mesters J. R., Barinka C., Li W., Tsukamoto T., Majer P., Slusher B. S., Konvalinka J. and Hilgenfeld R. (2006) Structure of glutamate carboxypeptidase II, a drug target in neuronal damage and prostate cancer. *EMBO J.* **25**, 1375–1384.

Morrison J. F. (1969) Kinetics of the reversible inhibition of enzyme-catalysed reactions by tight-binding inhibitors. *Biochim. Biophys. Acta.* **185**, 269–286.

Murphy G., Ragde H., Kenny G. *et al.* (1995) Comparison of prostate specific membrane antigen, and prostate specific antigen levels in prostatic cancer patients. *Anticancer Res.* **15**, 1473–1479.

Nan F., Bzdega T., Pshenichkin S., Wroblewski J. T., Wroblewska B., Neale J. H. and Kozikowski A. P. (2000) Dual function glutamate-related ligands: discovery of a novel, potent inhibitor of glutamate carboxypeptidase II possessing mGluR3 agonist activity. *J. Med. Chem.* **43**, 772–774.

Neale J. H., Olszewski R. T., Gehl L. M., Wroblewska B. and Bzdega T. (2005) The neurotransmitter N-acetylaspartylglutamate in models of pain, ALS, diabetic neuropathy, CNS injury and schizophrenia. *Trends Pharmacol. Sci.* **26**, 477–484.

Pangalos M. N., Neefs J. M., Somers M., Verhasselt P., Bekkers M., van der Helm L., Fraiponts E., Ashton D. and Gordon R. D. (1999) Isolation and expression of novel human glutamate carboxypeptidases with N-acetylated alpha-linked acidic dipeptidase and dipeptidyl peptidase IV activity. *J. Biol. Chem.* **274**, 8470–8483.

Pinto J. T., Suffoletto B. P., Berzin T. M., Qiao C. H., Lin S., Tong W. P., May F., Mukherjee B. and Heston W. D. (1996) Prostate-specific membrane antigen: a novel folate hydrolase in human prostatic carcinoma cells. *Clin. Cancer Res.* **2**, 1445–1451.

Renneberg H., Friedetzky A., Konrad L., Kurek R., Weingartner K., Wennemuth G., Tunn U. W. and Aumuller G. (1999) Prostate specific membrane antigen (PSM) is expressed in various human tissues: implication for the use of PSM reverse transcription polymerase chain reaction to detect hematogenous prostate cancer spread. *Urol. Res.* **27**, 23–27.

Robinson M. B., Blakely R. D., Couto R. and Coyle J. T. (1987) Hydrolysis of the brain dipeptide N-acetyl-L-aspartyl-L-glutamate. Identification and characterization of a novel N-acetylated alpha-linked acidic dipeptidase activity from rat brain. *J. Biol. Chem.* **262**, 14 498–14 506.

Schmidt B., Anastasiadis A. G., Seifert H. H., Franke K. H., Oya M. and Ackermann R. (2003) Detection of circulating prostate cells during radical prostatectomy by standardized PSMA RT-PCR: association with positive lymph nodes and high malignant grade. *Anticancer Res.* **23**, 3991–3999.

Sedo A., Malik R. and Krepela E. (1998) Dipeptidyl peptidase IV in C6 rat glioma cell line differentiation. *Biol. Chem.* **379**, 39–44.

Serval V., Barbeito L., Pittaluga A., Cheramy A., Lavielle S. and Glowinski J. (1990) Competitive inhibition of N-acetylated-alpha-linked acidic dipeptidase activity by N-acetyl-L-aspartyl-beta-linked L- glutamate. *J. Neurochem.* **55**, 39–46.

Silver D. A., Pellicer I., Fair W. R., Heston W. D. and Cordon-Cardo C. (1997) Prostate-specific membrane antigen expression in normal and malignant human tissues. *Clin. Cancer Res.* **3**, 81–85.

Slusher B. S., Vornov J. J., Thomas A. G. *et al.* (1999) Selective inhibition of NAALADase, which converts NAAG to glutamate, reduces ischemic brain injury. *Nat. Med.* **5**, 1396–1402.

Sokoloff R. L., Norton K. C., Gasior C. L., Marker K. M. and Grauer L. S. (2000) A dual-monoclonal sandwich assay for prostate-specific membrane antigen: levels in tissues, seminal fluid and urine. *Prostate* **43**, 150–157.

Subasinghe N., Schulte M., Chan M. Y., Roon R. J., Koerner J. F. and Johnson R. L. (1990) Synthesis of acyclic and dehydroaspartic acid analogues of Ac- Asp-Glu-OH and their inhibition of rat brain N-acetylated alpha- linked acidic dipeptidase (NAALA dipeptidase). *J. Med. Chem.* **33**, 2734–2744.

Troyer J. K., Beckett M. L. and Wright G. L. Jr (1995) Detection and characterization of the prostate-specific membrane antigen (PSMA) in tissue extracts and body fluids. *Int. J. Cancer* **62**, 552–558.

Tsai G., Dunham K. S., Drager U., Grier A., Anderson C., Collura J. and Coyle J. T. (2003) Early embryonic death of glutamate carboxypeptidase II (NAALADase) homozygous mutants. *Synapse* **50**, 285–292.

Tsukamoto T., Flanary J. M., Rojas C., Slusher B. S., Valiaeva N. and Coward J. K. (2002) Phosphonate and phosphinate analogues of N-acylated gamma-glutamylglutamate. Potent inhibitors of glutamate carboxypeptidase II. *Bioorg. Med. Chem. Lett.* **12**, 2189–2192.

Tsukamoto T., Majer P., Vitharana D. *et al.* (2005) Enantiospecificity of glutamate carboxypeptidase II inhibition. *J. Med. Chem.* **48**, 2319–2324.

Vitharana D., France J. E., Scarpetti D., Bonneville G. W., Majer P. and Tsukamoto T. (2002) Synthesis and biological evaluation of (R)- and (S)-2-(phosphonomethyl)pentanedioic acids as inhibitors of glutamate carboxypeptidase II. *Tetrahedron Asymmetry* **13**, 1609–1614.

Whelan J. (2000) NAALADase inhibitors: a novel approach to glutamate regulation. *Drug Discov. Today* **5**, 171–172.

Xiao Z., Adam B. L., Cazares L. H., Clements M. A., Davis J. W., Schellhammer P. F., Dalmasso E. A. and Wright G. L. Jr (2001) Quantitation of serum prostate-specific membrane antigen by a novel protein biochip immunoassay discriminates benign from malignant prostate disease. *Cancer Res.* **61**, 6029–6033.

Zhang W., Slusher B., Murakawa Y., Wozniak K. M., Tsukamoto T., Jackson P. F. and Sima A. A. (2002) GCPII (NAALADase) inhibition prevents long-term diabetic neuropathy in type 1 diabetic BB/Wor rats. *J. Neurol. Sci.* **194**, 21–28.

Zhou J., Neale J. H., Pomper M. G. and Kozikowski A. P. (2005) NAAG peptidase inhibitors and their potential for diagnosis and therapy. *Nat. Rev. Drug Discov.* **4**, 1015–1026.

